

## The stability of conjugate natural convection boundary layers

N. Williamson<sup>1</sup> and S. W. Armfield<sup>1</sup>

<sup>1</sup>School of Aerospace, Mechanical and Mechatronic Engineering, University of Sydney, NSW 2008, Australia

### Abstract

In this paper a previously unreported stability characteristic of coupled natural convection boundary layers is investigated. The flow is examined numerically here with simulations of two adjacent two-dimensional rectangular cavities joined along one vertical wall which has an infinite conductivity. The outer vertical walls are isothermal, with one ‘hot’ wall and one ‘cold’ wall and all horizontal walls are adiabatic. Heat is transferred between the cavities through the conducting wall so a natural convection cell forms in both cavities. The boundary layer formed on the ‘hot’ cavity side of the conducting plate flows downwards, while that on the ‘cold’ cavity side flows upwards, forming a conjugate boundary layer system.

Simulations have been conducted over the range  $Ra = 6 - 18 \times 10^9$  at a Prandtl number of 7.5. The interaction between the boundary layers that form on either side of the vertical conducting wall is of primary interest in this study. An uncoupled laminar natural convection boundary layer is known to be convectively unstable above  $Ra \approx 10^6$  at  $Pr = 7.5$  whereas the transition to absolute instability is known to occur above  $Ra \approx 10^{11}$ . In the present study the coupled system is shown to be absolutely unstable above  $Ra = 1.2 \times 10^{10}$ , with a weak dependence on cavity aspect ratio. Perturbations form in the boundary layers on both sides of the conducting wall and grow with the boundary layer. This flow configuration is of fundamental importance to many common heat and mass transfer problems.

### Introduction

Natural convection flows occur widely and are of interest in many engineering problems including solar collectors, nuclear reactors, electronic equipment and HVAC problems. Improved understanding of such flows may lead to better prediction and optimisation of heat transfer. The flow configuration considered here is that which occurs on either side of a conducting wall with a temperature difference across the wall. The problem is investigated via a dual cavity geometry, illustrated in figure 1. The left and right outer walls are held at fixed ‘hot’ and ‘cold’ temperatures respectively. The top and bottom walls are adiabatic and the central vertical wall has an infinite conductivity. Natural convection boundary layers form on the vertical walls which flow onto the horizontal walls forming intrusions. The direction of flow circulation is indicated in figure 1 by arrows. In the high Rayleigh number flow ( $Ra > 10^6$ ) considered here, the core of the cavities are nearly linearly stratified and the heat transfer occurs via a primarily convective mechanism [6]. The flow behavior depends on the Rayleigh number, Prandtl number and cavity aspect ratio  $A = H/W$ .

Earlier studies have highlighted the affect that partition walls have on mean heat transfer characteristics. Typically the results are correlated with a Nusselt number relation of the form  $Nu \sim Ra^{1/4}(N+1)^{-n}$  where  $n$  is a constant coefficient and  $N$  is the number of partition walls [1, 3, 9, 13, 12]. The parameter space covered by these studies is given in table 1. The transient start up characteristics of the partitioned cavity were examined in [13] but no unsteadiness was reported in the fully developed flow.

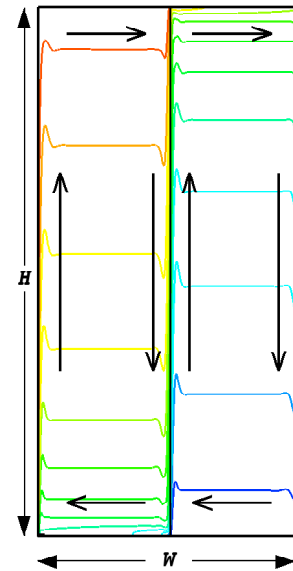


Figure 1: Configuration studied, with contours of mean temperature illustrated at  $Ra = 7 \times 10^9$  and  $A = 2$ . Arrows indicate flow direction inside the cavities.

	Pr	Ra	N	A
[1]	6	$10^9 < Ra < 10^{10}$	0-2	0.33
[3]	2700-7000	$10^4 < Ra < 10^6$	0-1	1
[9]	6	$10^8 < Ra < 10^{10}$	0-4	4
[12]	0.71	$10^5 < Ra < 10^7$	0-4	0.5-1.5
[13]	7	$1.8 \times 10^9$	0-1	1

Table 1: Previous partitioned cavity studies.

At a Rayleigh number  $Ra_c$ , a laminar natural convection boundary layer becomes convectively unstable, meaning that if a perturbation of frequency  $f_c$  is imposed on the flow, the signal will be amplified by the boundary layer. Once the exciting perturbation ceases the oscillations will decay back to the steady base-flow. The exact value of  $Ra_c$  depends on flow configuration details such as background stratification and wall boundary condition (isoflux or isothermal) but is generally above  $Ra \approx 10^6$  for  $Pr = 7$  [5, 2]. On an infinite vertical plate in an unstratified domain,  $Ra_c = 2.4 \times 10^5$  [8]. The critical Rayleigh number for convective instability of the boundary layers in isothermal cavity flow is  $Ra \approx 10^6$  for  $Pr = 7.5$  [2]. At a higher Rayleigh number,  $Ra_a > Ra_c$ , the boundary layer becomes absolutely unstable. Here any oscillations will persist and be self sustaining even if the initial exciting perturbation ceases.  $Ra_a$  is known to be greater than  $10^{11}$  for natural convection boundary layers.

Convectively unstable systems can become absolutely unstable if there is a reinforcing feedback mechanism. An example of such a mechanism is the flow in very high aspect ratio cavities where the horizontal walls are short and the two vertical walls are more directly connected. A perturbation can grow along one vertical boundary layer, then be advected horizontally through

the top or bottom intrusions onto the opposite vertical wall, where it is further amplified causing the cavity flow to bifurcate. For a high aspect ratio cavity Elder [4] found experimentally that travelling waves appeared at  $Ra = 5.6 \times 10^9$  with  $Pr = 7$  and  $A = 10 - 30$ . Using numerical simulations Le Quere [11] found the transition to unsteadiness occurred at  $Ra \approx 9 \times 10^9$  with  $Pr = 7$  and  $A = 10$ .

In a conjugate boundary layer, a feedback mechanism exists through the temperature field across the conducting plate. In this study it is shown that this coupling causes the boundary layers on either side of the conducting plate to become absolutely unstable at a lower Rayleigh number than if the conducting wall was isothermal. We use direct numerical simulations to locate the critical Rayleigh number for this flow configuration, investigate the mechanisms which drive this instability and the effect this has on cavity heat transfer characteristics.

### Numerical formulation

The two-dimensional Navier-Stokes equations for incompressible flow with the Oberbeck-Boussinesq approximation for buoyancy are,

$$\begin{aligned} \frac{\partial u_i}{\partial x_i} &= 0, \\ \frac{\partial u_i}{\partial t} + \frac{\partial(u_i u_j)}{\partial x_j} &= -\frac{\partial p}{\partial x_i} + \frac{Pr}{Ra^{1/2}} \frac{\partial^2 u_i}{\partial x_j \partial x_j} - Pr \phi, \\ \frac{\partial \phi}{\partial t} + \frac{\partial(u_j \phi)}{\partial x_j} &= \frac{1}{Ra^{1/2}} \frac{\partial^2 \phi}{\partial x_j \partial x_j}, \end{aligned}$$

where  $Pr$  is the Prandtl number, the Reynolds number is defined as  $Re = U^* H / \nu$  and the Rayleigh number is  $Ra = g \beta \Delta \theta H^3 / \nu \alpha$ .  $\nu$  and  $\alpha$  are the kinematic viscosity and thermal diffusivity of the fluid. The velocity ( $U_i$ ), temperature ( $\theta$ ), pressure ( $P$ ), time ( $T$ ) and length ( $X_i$ ) are made non-dimensional as  $u_i = U_i / U^*$ ,  $\phi = (\theta - \theta_r) / \Delta \theta$ ,  $p = P / \rho U^{*2}$ ,  $t = T U^* / H$  and  $x_i = X_i / H$  respectively.  $\Delta \theta = \theta_H - \theta_C$  is the temperature difference between the hot and cold walls and the reference temperature  $\theta_r = 0.5(\theta_H + \theta_C)$ . The characteristic velocity is obtained from  $U^* \sim \kappa Ra^{1/2} / H$  [10].  $H$  is the height of the cavity. The horizontal width  $W$  does not appear in the equations.

The discretised governing equations were solved in finite volume form on a non-staggered Cartesian grid. The spatial derivatives were discretised using second order central finite differences except for the advective terms which are discretised using the third-order accurate QUICK scheme [7]. The advective terms were advanced in time using the second order Adams-Bashforth scheme while the viscous terms were advanced using the Crank-Nicolson scheme. The system of equations was solved with the BICGSTAB solver with a Multi-grid Jacobi preconditioner.

We have performed a series of simulations over the range  $Ra = 0.6 - 1.8 \times 10^{10}$  at a Prandtl number of  $Pr = 7.5$  and with  $A = 1$  and  $A = 2$ . Grid independent solutions have been obtained at  $Ra = 1.4 \times 10^{10}$  with a grid size of  $\Delta x = 0.00005$  and  $\Delta y = 0.001$  and a time step of  $\Delta t = 7 \times 10^{-5}$ . The grid is uniform in the vertical ( $y$ ) direction and has 0.5-1% linear stretching in the horizontal ( $x$ ) direction giving  $n_y = 1029$  and  $n_x = 776$  computational nodes at  $A = 2$  and  $n_x = 1032$  at  $A = 1$ . The same grid is used for all other simulations.

An initial simulation was performed at  $Ra = 1.2 \times 10^{10}$  with the initial condition being a uniform temperature of  $\phi = 0$  with zero initial velocity. The simulation was continued until the flow reached full development and statistics are converged. Subsequent simulations at other Rayleigh numbers have been restarted from this fully developed flow field.

### Results

The development of the flow from an initial  $\phi = 0$  condition is given in figure 2 for  $Ra = 1.2 \times 10^{10}$  and  $A = 2$ . In this figure  $\phi$  is plotted with time at a location on the bottom left side of the conducting wall. For  $t < 3$  the boundary layers form on the hot and cold walls and flow onto the horizontal walls in the same manner described for isothermal cavity flow [10]. At  $t \approx 3$  the horizontal intrusions hit the vertical conducting wall and begin to fill up the interior of the cavities. By  $t = 70$  the cavity is stratified, but does not approach its final mean value until  $t > 300$ . While the cavity is unstratified, over  $t \approx 3 - 30$ , waves are generated by a hydraulic jump type mechanism in the downstream corners of the isothermal walls where the vertical boundary layers flow into the horizontal intrusions. These waves propagate across the cavity and along the conducting wall.

All the simulations in this study are well above  $Ra_c = 10^6$ , so the boundary layers are convectively unstable to waves with frequencies in the range  $f_1(y) - f_2(y)$ , where  $f_1$  and  $f_2$  vary with height or local Rayleigh number. The exact values of  $f_1$  and  $f_2$  are not known for the dual cavity or single cavity problem. Any perturbations to the boundary layers on both isothermal and conducting walls will be amplified if their frequencies are within this range.

At  $t = 30$ , the perturbations from the corners have ceased but the oscillations illustrated in figure 2 are self-sustaining and continue to grow on the conducting wall.

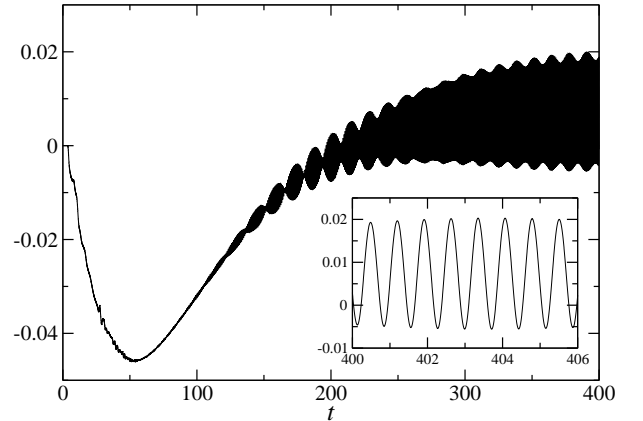


Figure 2: Time trace of  $\phi$  for  $Ra = 1.2 \times 10^{10}$  and  $A = 2$  at  $y = 0.1$  and  $\Delta x = 0.005$  left of the conducting wall.

The results over  $Ra = 0.6 - 1.0 \times 10^{10}$ , do not have this behavior. Regardless of any additional perturbations applied to the system, the oscillations in the conducting boundary layer eventually dissipate and a steady flow field is obtained. This indicates that the flow becomes absolutely unstable between  $Ra_a = 1.0 - 1.2 \times 10^{10}$  and that below  $Ra_a = 1.0 \times 10^{10}$  the boundary layers are only convectively unstable. Subsequent tests at  $A = 1$  show the critical Rayleigh number is slightly higher at this aspect ratio with  $Ra_a = 1.2 - 1.4 \times 10^{10}$ . At this stage it is not clear why the flow is more stable at a higher aspect ratio.

In figure 2, over  $t = 70 - 250$ , it is clear there are two frequencies of oscillation present, a high frequency wave with a period of  $t = 1.33$  and a low frequency wave with a period of  $t \approx 14$ . The high frequency signal is observed in all the simulations performed here and has a normalised frequency,  $f^* = f_c \nu^{1/3} / (g \beta \Delta \theta)^{2/3} = 0.0142$ . The wave velocity is  $U_w = 0.23 U^*$ , which is  $U_w \approx 1.2 V_m$ , where  $V_m$  is the maximum veloc-

ity in the boundary layer, inline with results in [2]. After  $t = 300$  the low frequency wave has dissipated significantly. Similar low frequency waves are observed when the Rayleigh number is suddenly changed in the simulations which are restarted from the fully developed  $Ra = 1.2 \times 10^{10}$  solution. This suggests the low frequency wave relates to a start-up disturbance with a period governed by the circulation time of the cavity which is approximately  $(2H + W)/U_w \approx 15.4$ . The period of the low frequency waves in the  $A = 1$  simulations is  $t \approx 30$ .

Time traces of  $\phi$  and the velocity components at other locations around the cavity (omitted here for brevity) show that the high frequency waves do not circulate around the cavity but are dissipated in the horizontal intrusions. The high frequency waves at the conducting plate persist and so it may be hypothesised that they are driven by some other mechanism. Examining the interaction of the waves across the conducting plate illustrates a potential mechanism. In figure 3 the temperature perturbation is shown on both sides of the plate and directly on the plate at time  $t = t_1$  (black lines) and a short time later at  $t = t_2$  (red lines). From halfway up the vertical plate, the waves on each side of the plate travel in the direction of flow and are strongly amplified. The temperature perturbation is apparently conducted through the plate to the boundary layer on the opposing side. On this opposite side, or equivalently at the upstream ends of the plate, the perturbations conducted through the wall are much larger than those in the boundary layer. Here the waves flow against the mean flow in the boundary layer as illustrated by the arrows in the inset log plot in figure 3. These waves are an illustration of the direct coupling between the two boundary layers and a possible feedback mechanism by which the system becomes absolutely unstable. An initial perturbation on one side of the plate would be amplified along one boundary layer, conducted through the plate, and then be amplified in the opposing direction in the other cavity. The perturbation will continually increase in amplitude until ultimately the growth of the waves in the system are limited by dissipation in the boundary layer.

An interesting additional test that was performed was to numerically instantly ‘turn off’ the conduction through the plate and replace the temperature on the plate with the local mean temperature. This has the effect of eliminating communication between the boundary layers. The waves then dissipate and the flow eventually reaches a steady state solution.

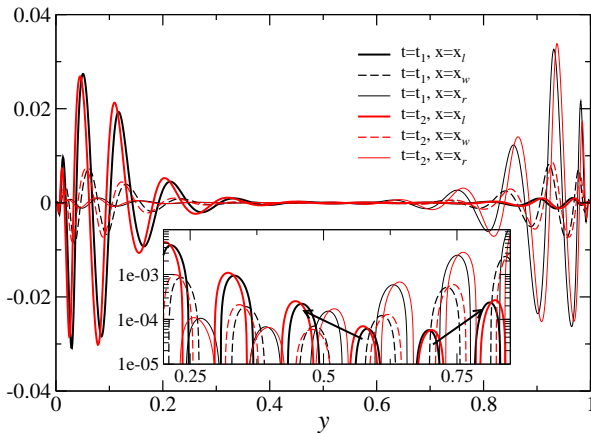


Figure 3:  $\phi'$  at  $Ra = 1.4 \times 10^{10}$  and  $A = 2$ , given at three horizontal locations:  $x_w$  at the conducting plate,  $x_l = x_w - 0.002$  just to the left of the plate and  $x_r = x_w + 0.002$  just to the right of the plate. The data is plotted against vertical location and presented at two time points,  $t_1$  and  $t_2 = t_1 + 0.07$  to show progression of the waves in the boundary layer. The inset plot is a log plot of the same data.

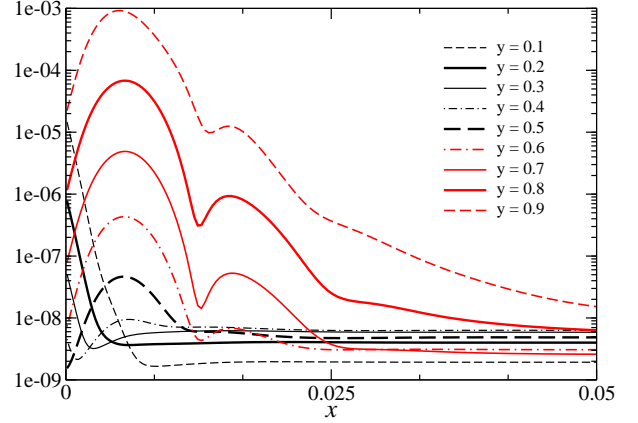


Figure 4:  $\langle \phi' \phi' \rangle$  at  $Ra = 1.4 \times 10^{10}$  and  $A = 2$  with distance from the conducting wall in the right cavity.

The growth of the temperature perturbations along the conducting plate boundary layers is illustrated in figure 4 where  $\langle \phi' \phi' \rangle$  is plotted with distance from the conducting wall in the right cavity. At the upstream end, for  $y < 0.4$ ,  $\langle \phi' \phi' \rangle$  peaks at the wall, evidence of the perturbation transmitted through the plate. At  $y > 0.4$  the temperature fluctuation peaks in the boundary layer.

The coupling between the boundary layers across the plate is also clearly illustrated by the the transport equation for the temperature variance  $\langle \phi' \phi' \rangle$  which is given as,

$$0 = \underbrace{-\langle u_i \rangle \frac{\partial \langle \phi' \phi' \rangle}{\partial x_i}}_A - 2 \underbrace{\langle u_i' \phi' \rangle \frac{\partial \langle \phi \rangle}{\partial x_i}}_P - \underbrace{\frac{2}{Ra^{1/2}} \langle \frac{\partial \phi'}{\partial x_i} \frac{\partial \phi'}{\partial x_i} \rangle}_D + \underbrace{\frac{1}{Ra^{1/2}} \frac{\partial^2}{\partial x_i^2} \langle \phi' \phi' \rangle}_V. \quad (1)$$

The convection, production, dissipation and viscous diffusion balance terms are labelled  $A$ ,  $P$ ,  $D$  and  $V$  respectively. The turbulent diffusion terms are neglected from the above balance as they are negligibly small in this flow. The balance terms are plotted in figure 5 (a-b) illustrating how the perturbation is diffused through the conducting plate from the downstream, high amplitude end of the boundary layer to the upstream, low amplitude end of the other boundary layer. At  $y = 0.2$ , the upstream end of the right side boundary layer, diffusion dominates with maximum value adjacent to the conducting plate, balanced by the dissipation term. Production is negligible. At  $y = 0.8$ , the production term dominates and is much greater than the diffusion of the perturbation through the conducting wall.

The turbulent kinetic energy balance is not shown for brevity here but we can report that the velocity perturbation is driven by buoyancy across the height of the plate. Shear production is negligible at the upstream ends of the plate and slightly dissipative at the downstream ends. This is typical of high Prandtl number natural convection boundary layers [5].

The mean heat transfer across the cavity is illustrated in figure 6 where the Nusselt number is plotted normalised by  $Ra^{1/4}$ , the high Rayleigh number scaling relation given in [10]. Nishimura *et al.* [9] found  $Nu_H = 0.297 Ra^{1/4} (N + 1)^{-1}$  with experiments and simulations over the range  $10^8 < Ra < 10^{10}$  where  $Nu_H = QH/\alpha \Delta T$ . Our results are obtained using  $Nu_H = d\phi/dx|_{x=0}$ . With one partition ( $N = 1$ ), the constant obtained from Nishimura *et al.* is  $Nu_H/Ra^{1/4} = 0.148$  where

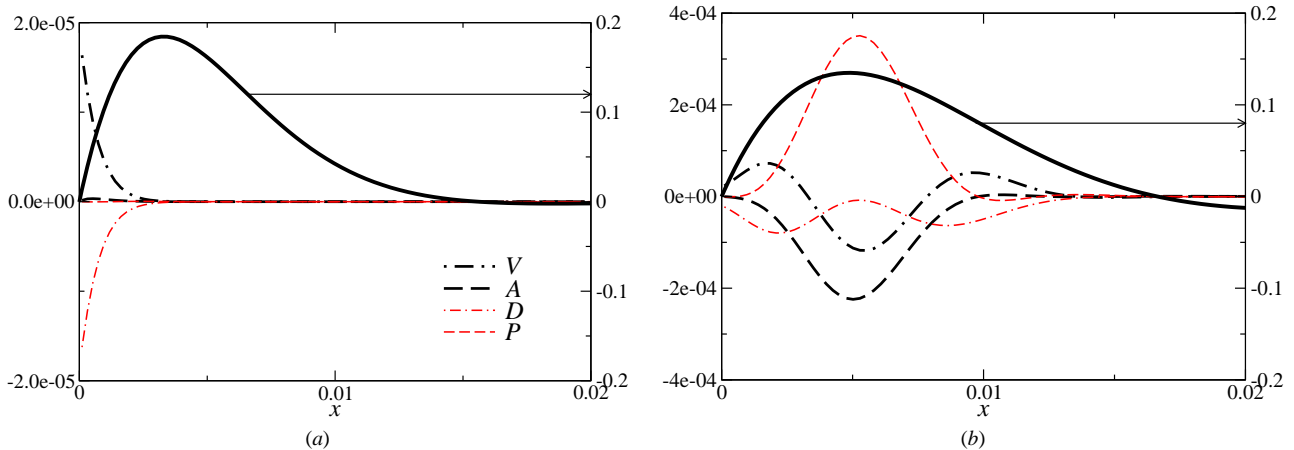


Figure 5: Budget for the temperature variance with distance from the conducting plate in right cavity at  $y=0.2$  (a) and  $y=0.8$  (b) for  $Ra = 1.4 \times 10^{10}$  with  $A = 2$ . Legend for budgets is given in (a) with reference to equation (1) and the thick black line gives mean vertical velocity at those locations.

as the present simulations are approximately 5% higher at  $Nu_H / Ra^{1/4} = 0.155$ . There does not appear to be a large jump in the heat transfer between the steady/unsteady regimes between  $Ra = 1.0 - 1.2 \times 10^{10}$  for  $A = 2$  and  $Ra = 1.2 - 1.4 \times 10^{10}$  for  $A = 1$ .

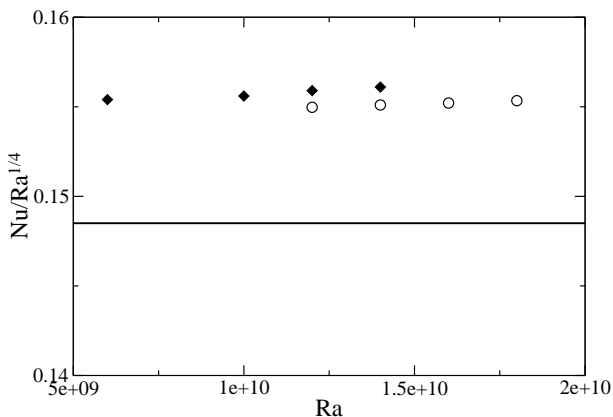


Figure 6: Nusselt number results presented for  $A = 2$  (diamonds) and  $A = 1$  (circles). Solid line indicates the constant from [9] with  $N = 1$ .

## Conclusions

The natural convection boundary layer which is formed on either side of a conducting plate in a square cavity is shown to become absolutely unstable at a Rayleigh number lower than would occur if the plate was isothermal. The evidence presented suggests that the instability is a result of the thermal coupling between the natural convection boundary layers on either side of the plate which provides a feedback mechanism sufficient to produce an absolutely unstable system. The critical Rayleigh number for absolute instability is between  $Ra = 1.0 - 1.2 \times 10^{10}$  for  $A = 2$  and  $Ra = 1.2 - 1.4 \times 10^{10}$  for  $A = 1$ . The bifurcation is manifested as a single mode of oscillation with  $f^* = 0.0142$ . The mean heat transfer is well predicted by the empirical correlation of Nishimura *et al.* [9].

## References

[1] Anderson, R. and Bejan, A., Heat transfer through single and double vertical walls in natural convection: The-

ory and experiment, *Int. J. Heat Mass Transfer*, **24**, 1981, 1611 – 1620.

[2] Armfield, S. and Janssen, R., A direct boundary-layer stability analysis of steady-state cavity convection flow, *Int. J. Heat Fluid Flow*, **17**, 1996, 539 – 546.

[3] Cuckovic-Dzodzo, D. M., Dzodzo, M. B. and Pavlovic, M. D., Laminar natural convection in a fully partitioned enclosure containing fluid with nonlinear thermophysical properties, *Int. J. Heat Fluid Flow*, **20**, 1999, 614 – 623.

[4] Elder, J. W., Turbulent free convection in a vertical slot, *J. Fluid Mechanics*, **23**, 1965, 99–111.

[5] Gill, A. E. and Davey, A., Instabilities of a buoyancy-driven system, *J. Fluid Mechanics*, **35**, 1969, 775–798.

[6] Henkes, R. and Hoogendoorn, C., Scaling of the laminar natural-convection flow in a heated square cavity, *Int. J. Heat Mass Transfer*, **36**, 1993, 2913 – 2925.

[7] Leonard, B. P., A stable and accurate convective modelling procedure based on quadratic upstream interpolation, *Comp. Meth. Appl. Eng.*, **19**, 1979, 59–98.

[8] Nachtshiem, P. R., Stability of free convection boundary layer flows, *NASA TN D-2089*.

[9] Nishimura, T., Shiraiishi, M., Nagasawa, F. and Kawamura, Y., Natural convection heat transfer in enclosures with multiple vertical partitions, *Int. J. Heat Mass Transfer*, **31**, 1988, 1679 – 1686.

[10] Patterson, J. and Imberger, J., Unsteady natural convection in a rectangular cavity, *J. of Fluid Mech.*, **100**, 1980, 65–86.

[11] Quééré, P. L., Transition to unsteady natural convection in a tall water-filled cavity, *Phys. Fluids*, **2**, 1990, 503–515.

[12] Turkoglu, H. and Yuçel, N., Natural convection heat transfer in enclosures with conducting multiple partitions and side walls, *Heat Mass Transfer*, **32**, 1996, 1–8.

[13] Xu, F., Patterson, J. C. and Lei, C., Heat transfer through coupled thermal boundary layers induced by a suddenly generated temperature difference, *Int. J. Heat Mass Transfer*, **52**, 2009, 4966 – 4975.